International Journal of Biological Macromolecules 370 (2026) 152622

Contents lists available at ScienceDirect

International Journal of Biological Macromolecules

journal homepage: www.elsevier.com/locate/ijbiomac

Phosphate anions-induced liquid-liquid phase separation in silk fibroin systems to produce biologically stable patches

Rocco Malaspina [a], Martina Alunni Cardinali [b], Danila Maltsev [c], Valeria Libera [a], Alessia Pepe [d], Lucia Comez [e], Cristiano De Michele [f], Caterina Petrillo [a], Alessandro Paciaroni [a], Paola Sassi [b], Luca Valentini [c,*]

[a] Department of Physics and Geology, University of Perugia, Via A. Pascoli, 06123, Perugia, Italy
[b] Department of Chemistry, Biology and Biotechnology, University of Perugia, Via Elce di Sotto 8, 06123, Perugia, Italy
[c] Civil and Environmental Engineering Department, University of Perugia, Strada di Pentima 4, 05100, Terni, Italy
[d] Link Campus University, Department of Life Sciences, Health and Health Professions, Via del Casale di San Pio V 44, 00165, Roma, Italy
[e] Centro Nazionale delle Ricerche (CNR)—Istituto Officina dei Materiali (IOM), Unità Perugia, Via Alessandro Pascoli, 06123, Perugia, Italy
[f] Department of Physics, University of Rome La Sapienza, Piazzale Aldo Moro 2, 00185, Rome, Italy

ARTICLE INFO

Keywords:
Silk fibroin
Liquid-liquid phase separation
Coarse-grained modeling
Phosphate anions
Hydrophobic interactions

ABSTRACT

Silk fibroin (SF), the primary protein component of *Bombyx mori* silkworm cocoons, undergoes liquid–liquid phase separation (LLPS), followed by coacervation into fibers, in the silkworm glands. The molecular mechanisms underlying LLPS remain to be revealed. Here, we show that phosphate buffer (PB), a less commonly utilized, but more biomimetic route towards triggering SF assembly, induces LLPS of water-soluble SF by increasing hydrophobic interactions between SF chains. We demonstrate the ability of phosphate anions to promote self-assembly of silk fibroin through LLPS, resulting in protein-rich droplets. Complementary computational modeling using a bead-spring representation of SF supports the experimental findings and confirms the mechanistic origin of the assembly transitions, as driven primarily by hydrophobic interactions. FTIR spectroscopy was used to investigate structural differences upon LLPS between the dense and light phases, which were shown to be comprised mainly of random coil. After evaporation of the solvent, SF agglomerates were incorporated within the continuous silk matrix. This spatial confinement of solid droplets was stabilized by treatment with ethanol solution, promoting β-sheet formation via protein backbone dehydration. The material formulation was, finally, tested in simulated biological fluids (e.g., gastro-intestinal tract, based on European Pharmacopeia 9.0), highlighting the pH-dependent swelling, and overall stability of the films.

1. Introduction

Natural silk fibroin (SF) [1,2], a protein derived from the threads spun by *Bombyx mori* silkworm, contains a complex network of non-covalent hydrogen bonds, resulting in a multiscale organization of protein segments. Under certain conditions, this protein undergoes self-assembly, transitioning from a soluble protein with predominantly random coil secondary structure to β-sheets-rich insoluble material [3–7]. This structural transition drew the attention of researchers aiming to develop processes for conversion of silk into advanced materials [8–11]. Indeed, SF is often recognized for its biocompatibility, biodegradability, and excellent mechanical properties [12–17].

Liquid-liquid phase separation (LLPS) is the spontaneous demixing of an initially homogeneous solution into two (or more) distinct liquid phases. Both phases contain the solvent and solute, albeit at different concentrations; LLPS is considered one of the possible mechanisms of natural silk spinning [18] and is receiving great attention as a biomimetic approach to produce advanced materials. However, the critical questions of how SF undergoes LLPS under varying environmental conditions inside the silk glands, and how SF coacervates convert into the solid phase, remain unanswered.

Observing the natural *B. mori* silk spinning process, it was clarified that liquid silk phase separation is affected by various factors, such as metal ions concentration and pH [19,20]. The former plays a crucial role in *B. mori* silk glands, regulating the LLPS formation. The pH, changing throughout the spinning process, triggers silk fibroin self-assembly: from

* Corresponding author.
E-mail address: luca.valentini@unipg.it (L. Valentini).

https://doi.org/10.1016/j.ijbiomac.2026.152622
Received 13 February 2026; Received in revised form 15 May 2026; Accepted 18 May 2026
Available online 20 May 2026

a random-coil-rich soluble protein, to a β-sheet-rich fiber.

Phosphate anions [7] have been found to play a role in promoting β-sheet formation of spidroins during spider silk spinning. Moreover, it has already been reported that phosphate salts can induce LLPS in both native and recombinant spider silk proteins [21–23]. This fact is generally regarded as a consequence of the salting-out effect, and this is also consistent with findings regarding silkworm silk, where kosmotropic ions have been shown to influence phase separation [20,23]. The favorable interaction of phosphate with water [24–27] disrupts the proteins hydration layer and promotes intra- and inter-protein interactions. Furthermore, potassium phosphate has been used to prepare silk fibroin particles for drug delivery [7] and, more recently, it was reported that mild phosphate buffer can trigger self-assembly of silk proteins at a solid–liquid interface [28–31]. Moreover, hydrophobic and Hofmeister effect are believed to be strictly correlated. For example, Besford et al. [32] demonstrated by theory and molecular dynamics simulation a directly link between the rotational correlation of water molecules around an ionic co-solute and the perturbation of water structure, which ultimately leads to the hydrophobic interactions. The connection between hydrophobicity and salting-out effect is shown also for silk proteins, as different silk sequences with different hydrophobicity levels undergo LLPS in presence of different salts. More hydrophobic residues-rich sequences need less kosmotropic, or even mildly chaotropic, salts [18,23]. Even though a full description of the driving forces underlying LLPS in silk proteins would involve multiple mechanisms, the modulation of hydrophobic interactions, controlled by ions in the solution, plays an important role.

In general, protein microparticles formed through LLPS are reversible and tend to redissolve upon rehydration or dilution in aqueous media unless they undergo additional stabilization. Post-processing treatment in organic solvents, like ethanol or methanol, is commonly used to induce changes in secondary structure of SF, leading to perceptibly higher stability [24,27,29,30]. In particular, the use of ethanol for post-treatment is advantageous, compared to alternatives, because it does not leave traces in the material after evaporation and can be used to sterilize SF.

Additionally, when SF is formulated as particles, due to their enhanced absorption capacity, this biomaterial becomes an interesting vehicle, capable of transporting and delivering a wide range of bioactive molecules [28,31,33–35]. The ability of SF particles to load high amounts of bioactive molecules and protect them during the early stages of digestion is advantageous for oral administration in pharmaceutical and biomedical applications. Therefore, it is essential to investigate the stability of LLPS-produced SF particles in simulated body fluids.

Despite the increasing recognition of liquid–liquid phase separation (LLPS) as a key mechanism in natural silk spinning, several fundamental aspects remain unresolved. In particular, it is still unclear how specific environmental cues, such as ionic composition, drive silk fibroin (SF) coacervation, how the resulting liquid droplets evolve structurally, and how these, typically meta-stable, assemblies can be converted into mechanically and biologically robust solid materials.

Herein, we address these open questions by exploiting phosphate-mediated LLPS of SF as a biomimetic route to fabricate stable protein-based films. We demonstrate that phosphate ions effectively induce SF coacervation, generating liquid droplets that can be retained within a continuous protein matrix. By combining sequential LLPS with a post-casting ethanol treatment, we elucidate how ethanol-driven dehydration promotes β-sheet formation and stabilizes the coacervate-derived structures.

Furthermore, we integrate experimental observations with a coarse-grained (CG) simulation model that captures both intra- and intermolecular interactions of SF [34,35], successfully reproducing the experimental phase behavior and providing mechanistic insight into the self-assembly process. Overall, this work clarifies the role of phosphate-induced LLPS in SF organization and establishes a controlled strategy to translate transient liquid assemblies into robust films with enhanced stability in simulated biological fluids.

2. Experimental section

2.1. Materials

All chemicals used were of analytical grade. SF aqueous solution (50 mg/mL), potassium dihydrogen phosphate (KH_2PO_4) and potassium hydrogen phosphate (K_2HPO_4), as well as 1,6-hexanediol (HDO), hydrochloric acid (HCl), absolute ethanol (EtOH) and urea were purchased from Merck (Merck KGaA, Darmstadt, Germany) and used without further purification. Adenosine triphosphate (ATP) was supplied by the Department of Medicine and Surgery of the University of Perugia.

2.2. Preparation of PB-silk fibroin aqueous solutions and determination of the phase diagram

A stock solution of 0.75 M potassium PB at pH 7 was prepared. From that, PB solutions of 0.25 M, 0.375 M, 0.5 M, 0.625 M, were obtained by diluting with deionized water. In the same way, the commercial SF solution (50 mg/mL as reported by the manufacturer and further confirmed by weighing the solution after drying) was thinned with deionized water for lower concentrations, from 2 to 40 mg/mL.

Determination of the occurrence of LLPS in mixed SF/PB systems was carried out by injecting 20 μL of PB solution under the surface of 100 μL of SF solution. Post-mixing, we refer to the concentrations of SF and PB, as they are in combined solutions. As such, for instance, 50 mg/mL of SF becomes 42 mg/mL, and 0.75 M of PB becomes 0.13 M. The final-concentration nomenclature is maintained from here on and is preserved for films derived from corresponding mixtures.

The phase diagram was defined by going through the above-mentioned SF and PB concentration ranges. LLPS presence in each case was validated by optical microscopy (HRX-01, Hirox Co. Ltd., Tokyo, Japan). The data points in the phase separation map are classified visually into two groups: □ - no LLPS observed, and ○ - LLPS present.

2.3. Turbidity using UV–Vis spectroscopy

The turbidity of the SF solution upon addition of PB was monitored as a sign of phase separation. It was performed by means of a UV–Vis Jasco V-570 (Jasco Corporation, Tokyo, Japan) spectropolarimeter. Samples with pure SF (4 mg/mL) and SF 4 mg/mL + PB, with concentration ranging from 0.04 M to 0.13 M, were prepared. Each sample was then poured in a 1 mm path length quartz cell and the absorbance of the sample at 600 nm was recorded.

2.4. Circular dichroism

Analysis of SF conformation in solution was performed by Circular Dichroism. Measurements were carried out on a Jasco J-810 spectropolarimeter. Quartz cells with a pathlength of 0.01 mm were used and SF was diluted to 4 mg/mL, in order to get a definite signal from the protein while avoiding saturation. Measurements were taken both with and without the addition of 0.13 M PB. CD spectra of the solvents, pure water in the case of SF and 0.13 M PB in the case of SF + PB, were acquired too. Each spectrum was taken in the 190–350 nm range and established after the average of 3 accumulations.

2.5. Fluorescence recovery after photobleaching

Fluorescence recovery after photobleaching (FRAP) experiments were performed using a Nikon A1R+ laser-scanning confocal microscope (Nikon, Japan). A combination of 488/561 nm lasers was used for photobleaching at maximum intensity (100%), to ensure the sample excitation with the 488 nm source and the fluorescence recovery with the 561 nm one. All measurements were conducted with a 20× NA 0.7

Nikon Plan-Apo objective. The confocal pinhole was set to 1.7 Airy units, and images were recorded at a resolution of 512 × 512 pixels.

A circular region of interest (ROI) with a nominal radius of 1 μm was selected for photobleaching, corresponding to an approximate area of around 3 μm^2. Fluorescence recovery was monitored over time using the NIS-Elements AR software (Nikon). All experiments were performed at a controlled temperature of 20 °C.

Samples for FRAP analysis were prepared by dissolving the rhodamine B probe directly into the system. The LLPS solution was placed onto a glass slide, covered with a 24 × 24 mm^2 coverslip, and gently blotted to remove excess solution.

For image acquisition, four pre-bleach frames (~4 s total) were collected and averaged to normalize fluorescence intensity. The bleaching step consisted of three consecutive frames (~3 s). Recovery dynamics were then recorded over approximately 75 frames, corresponding to a total post-bleach acquisition time of ~130 s.

2.6. Computational modeling

Monte Carlo simulations were performed to gain insight into the molecular mechanisms leading to phase separation in SF systems. Silk fibroin chains were simulated with an extremely coarse-grained, bead-spring model, as it had already been done by other authors with other proteins [33,36]. A key feature in designing coarse-grained models for proteins is their molecular weight as the coacervation conditions typically depend on the chain length. Silk proteins are no exception in this regard, as they are composed of highly hydrophobic, repetitive regions that act as stickers and shorter, polar regions that act as linkers [18,37]. Both valence and patterning of residues in the protein chains have been shown, by both experiments and simulations, to be critical in controlling saturation concentration [38]. Our model was designed to reproduce the features of SF heavy chain. The native SF molecular weight, as found by genome sequencing of the silkworms and confirmed by extracting the solubilized protein directly from the insect's glands, is 390 kDa [39]. However, the chain is typically hydrolyzed during the regeneration of fibers, yielding a broad molecular weight distributions [38]. The native sequence of SF heavy chain consists of 12 repetitive regions interspersed with 11 linkers [37]. Our regenerated SF has an average molecular weight, reported by the manufacturer, of 100 kDa, about a quarter of the native SF molecular weight. Consequently the model was developed with a total of 3 repetitive regions connected by 2 linker sequences.

Each repetitive part is represented by a bead, which we will refer as B (which stands for blue). The linker regions are modelled by a sequence of three smaller beads. This choice was made to better represent the dynamic nature of the linkers and to introduce a term able to replicate the interactions among aromatic residues, present in the central part of these sequences. Indeed, interaction among aromatic residues, the latter having been shown to be important in phase separation of proteins [18,40]. So, the linkers are depicted by a Y-R-Y sequence, where Y stands for yellow and R for red; the R beads contain the aromatic part. B beads were assigned a diameter of $\sigma_B = 2$ nm, while for R and Y we set $\sigma_R = \sigma_Y = 1$ nm.

Since all the experimental characterizations were performed at room temperature, every parameter in the model with dimensions of energy was expressed as multiple of k_BT. The interactions between beads are divided into two categories: bonded and non-bonded. The former are, in turn, of two different types: finitely extensible nonlinear elastic (FENE) attractions between consecutive beads, and bending potentials between consecutive bonds.

The form of the FENE potential between consecutive beads i and j (so, i,j = B,Y,R) is the following:

$$V_{ij}^{FENE} = -\frac{1}{2}\varepsilon_{FENE} r_{max}^2 \ln\left(1 - \left(\frac{r_{ij}}{r_{max}}\right)^2\right)$$

where r_{ij} is the distance between the centers of beads i and j. Maximum bond length was set to be $r_{max} = 1.2\sigma_{ij}$, with σ_{ij} being the average diameter of beads i and j, and $\varepsilon_{FENE} = 1.0\ k_BT/nm^2$.

The bending potential between bonds I and J is expressed as:

$$V_{IJ}^{bend} = \frac{1}{2}\kappa_{bend}(1 - cos\theta_{IJ})$$

where θ_{IJ} is the angle between consecutive bonds, and $\kappa_{bend} = 1.0\ k_BT$.

The non-bonded attractive interactions, which are responsible for the phase separation, were set to be homotypical: B beads interact only with other B beads and R beads only with other R beads, as has been proven to be the case for silk proteins [18], while there is no Y—Y attraction as the Y beads are representative of non-aromatic parts of the linkers that do not have substantial role in the phase separation. A truncated Lennard-Jones potential was used, which explicit form is:

$$V_i^{nb}(r) = \begin{cases} 4\varepsilon_i\left[\left(\frac{\sigma_i}{r}\right)^{12} - \left(\frac{\sigma_i}{r}\right)^{6} - \left(\frac{1}{2.5}\right)^{12} + \left(\frac{1}{2.5}\right)^{6}\right] \text{ if } r \le 2.5\sigma_i \\ 0 \text{ if } r > 2.5\sigma_i \end{cases}$$

where r is the distance between the centers of the two beads and i = B,R. The simulations were run with different ε_B values, while keeping $\varepsilon_B/\varepsilon_R = 2$. Among the remaining pairs of beads, a Weeks-Chandler-Anderson (WCA) repulsion potential was used to simulate the excluded-volume effect:

$$V_{ij}^{WCA}(r) = \begin{cases} 4\varepsilon_{rep}\left[\left(\frac{\sigma_{ij}}{r}\right)^{12} - \left(\frac{\sigma_{ij}}{r}\right)^{6}\right] \text{ if } r \le \sigma_{ij} \\ 0 \text{ if } r > \sigma_{ij} \end{cases}$$

where i,j = Y,B,R, σ_{ij} is the same as previously defined and $\varepsilon_{rep} = 1.0\ k_BT$.

The Monte Carlo simulations were performed with 450 SF chains in a cubic box, with dimensions defined to match the experimentally tested concentration of SF.

2.7. Production of SF and SF/PB films and ethanol stabilization

Films were obtained from aqueous SF and mixed SF/PB solutions. To specify, 120 μL of a solution would be deposited on a glass slide, and the film would subsequently form upon evaporation of the solvent, at ambient conditions. To stabilize the SF and SF/PB films, a 70% v/v solution of ethanol in water was utilized. The films were placed inside a glass Petri dish, and 3 mL of ethanol solution were dropped, fully covering the sample. The treatment was carried out for 2 hours. After that, the films were taken out with tweezers and placed on a clean Petri dish to dry at room temperature.

2.8. Micro-FTIR characterization of LLPS films

Determination of the SF conformation in dried films was carried out using micro-Fourier transform infrared (micro-FTIR) spectroscopy in transmission mode. Measurements were performed at two different SF concentrations presented in the Phase Diagram, with and without addition of PB. The concentrations utilized were: 42 mg/mL SF, 8 mg/mL SF, 42 mg/mL SF + 0.13 M PB, 8 mg/mL SF + 0.13 M PB; analysed both before and after ethanol stabilization. Data were collected using Bruker Tensor 27 spectrometer coupled with a Hyperion 3000 microscope (Bruker Optics GmbH & Co. KG, Ettlingen, Germany), equipped with 15X Cassegrain objective and 64 × 64-pixel focal plane array detector.

A total of 15 μL of the solution was deposited onto a CaF_2 window. From each sample, 3 maps, each consisting of 4096 spectra, were acquired. Out of those, 500 spectra (per specimen) were selected as the reference for SF secondary structure analysis. The selection was carried out using an in-house Python script, to pick the spectra with the best signal-to-noise ratio. The second derivative of each spectrum was

calculated, followed by vector normalization, and the analysis of the protein secondary structure was carried out looking at the negative minima of the second derivative, particularly focusing on the content of β-sheets and disordered structures (random coils, turns).

The second derivative approach has some upsides, as it prevents artifacts in the spectra that could arise from the baseline correction. Moreover, it better separates the Amide *I* and II contributions, thus facilitating the extraction of secondary structure components. Negative intensities of the peak can be directly associated with the species' concentrations; this way the intensity of the minima in the second derivative can be used in place of total area of the bands in the absorbance spectrum to estimate the sample composition. Assignments of the spectral components were performed following the protocol described by Belton et al. [41].

2.9. Degradation experiment in simulated body environments

Behavior of SF and SF + PB films was studied in simulated gastric and intestinal environments. To specify, the former was approximated with 0.1 M HCl solution, while the latter - with 0.1 M potassium phosphate buffer at pH 6.8. SF and SF + PB films were weighed and then exposed to the simulated body fluids. Tests at 2, 4, 8, 16, 24 and 48 h were performed. For each test, the film was weighed and subsequently immersed in the fluid for the corresponding amount of time, then it was taken out of the solution and let dry on air at room temperature. After 30 min of drying, the film was weighed again to quantify the mass change. For each condition, the degradation test was repeated three times. The films studied, both in gastric and intestinal environment, were SF 42 mg/mL and SF 42 mg/mL + PB 0.13 M. There were two sets of films of each composition—one that had not undergone the ethanol treatment, and one that had—so, 4 films in total.

3. Results and discussion

As mentioned above, LLPS of spider silk has been known to get triggered by phosphate anions [23,42], thus hinting at a potential role of phosphate in LLPS of *B. mori* SF. Before adding phosphate, the SF solution was transparent (Fig. 1a). However, it immediately turned turbid upon PB injection. When the mixture was observed under optical microscope, the formation of coacervates was clear (Fig. 1b). These findings were confirmed by turbidity experiments performed on SF and SF + PB solutions, where the optical density of the system was measured as function of PB concentration. The results corroborate phase separation when PB concentration exceeds a critical threshold (Fig. 1c). Depending on the concentrations of SF and PB, mixed solutions exhibited two distinct states: 1) a turbid LLPS solution with 2 phases clearly present - the dense phase in droplets and the light phase of the solution itself, 2) a transparent solution with no droplets (the only artifacts visible are solid SF aggregates). Delayed LLPS, mentioned in literature [20], has not been witnessed in our study, as we verified by measuring optical density of the solution for several minutes (Supplementary information, Fig. S1).

The liquid-like nature of the droplets was assessed by means of optical microscopy, as coalescence events between droplets were observed (Supplementary information, Movie S1), as well as by FRAP experiments. This latter technique relies on the assumption that photobleached molecules within the droplet can diffuse away from the bleached region and be replaced by unbleached fluorescent molecules, leading to fluorescence recovery over time [20,43].

First, a qualitative analysis shows that the sample prepared using rhodamine B exhibits an increasing intensity of red fluorescence within the dense phase particles, indicating that the probe was successfully loaded into the liquid condensates (Fig. 2a).

We then performed photobleaching experiments. A circular region with a radius of 1 μm within the droplet was selectively photobleached (Fig. 2b). A complete recovery of fluorescence was observed, consistent with dynamic, liquid-like behavior.

As a control, a different sample was dried prior to photobleaching. Under these conditions, where the droplets no longer exhibit liquid-like properties, no fluorescence recovery was recorded (Fig. 2c).

A phase separation map was generated (Fig. 3a) based on microscopy observations, determining the concentration of SF and PB under which SF undergoes LLPS.

The effect of SF and PB concentrations on the size of dense phase droplets was investigated. It was found that across the range of concentrations considered, the droplets average diameter remained in the interval of 4–6 μm, with fluctuating variation (Fig. 3b). However, it was confirmed with single-factor ANOVA test that the diameters were meaningfully different ($F = 152$ with F_{crit} of 1.5).

There appears to exist a concentration of PB, at about 0.08 M, that is conducive to a share of droplets with size in the range of 10–20 μm (hence, the wider standard deviation for those).

Different studies have suggested that anions play an important role in the silk spinning of spiders [42,44]. Since in the present case the addition of phosphate ions induces LLPS in SF, we suggest that, akin to what was reported for spidroin, hydrophobic interactions are likely important factors in the LLPS of SF.

To verify this hypothesis, we investigated the effect on our samples of different compounds, in order to get insight into the mechanism underlying the LLPS of the SF protein. 1,6-hexanediol (HDO), widely reported in the literature as a disruptor of weak hydrophobic interactions [20,45,46], was added. NaCl and ATP were also selected as electrostatic probes, and urea as hydrogen bond disruptor [47–49]. The addition of 10% HDO to our SF/PB solution in LLPS-state led to swift disappearance of the droplets (Fig. 3c). This finding proves the fundamental role of hydrophobic interactions in the formation of phosphate-induced LLPS of silk fibroin.

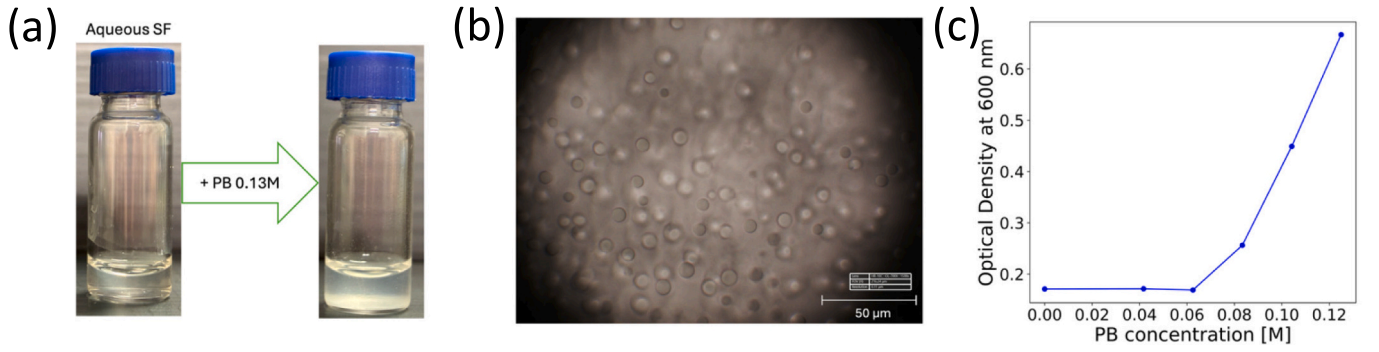

Fig. 1. LLPS behavior of SF and phosphate mixtures. (a) SF aqueous solution became turbid upon adding phosphate. (b) Micrographs of LLPS systems in liquid phase. Concentrations of SF and PB are respectively 42 mg/mL and 0.13 M. (c) Turbidity measurements, showing increase in optical density of the solution after addition of PB. The concentration of SF was 4 mg/mL.

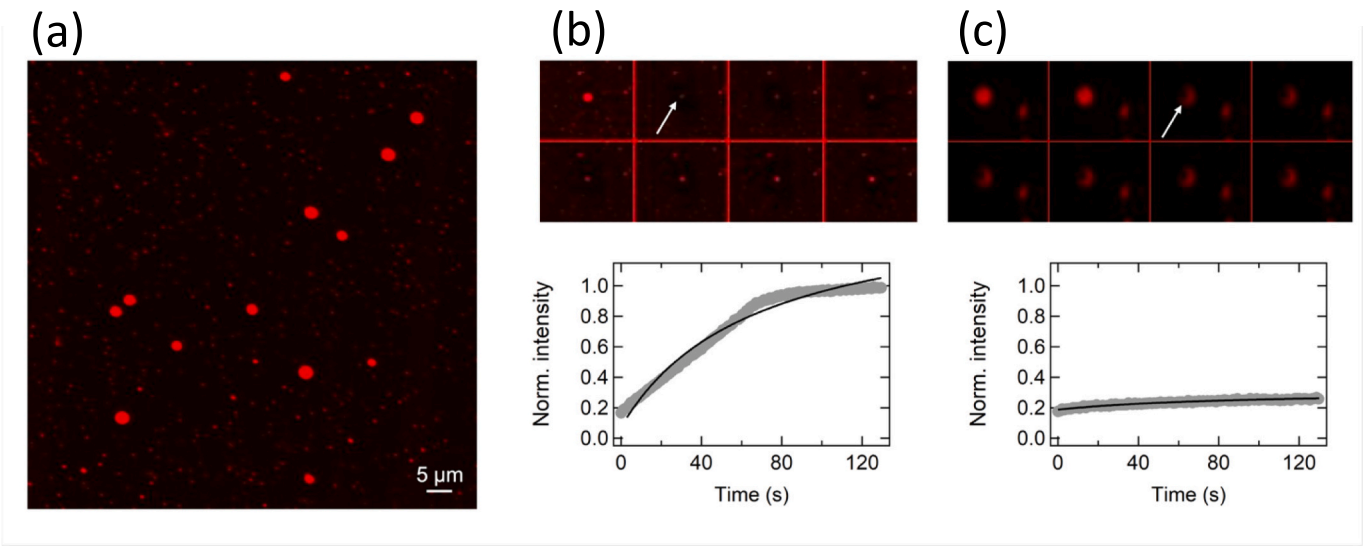

Fig. 2. SF phase separation was tested with fluorescence microscopy. (a) Micrograph obtained with Rhodamine B-labelled SF, showing the formation of the droplets. (b-c) Micrographs obtained from FRAP experiment (upper panels: 8 frames obtained before and after photobleaching, from left to right and top to bottom) and normalized intensity of fluorescence over time (lower panels) of SF + PB liquid (b) and dried (c) sample. The white arrows indicate the sample regions where the photobleaching occurred.

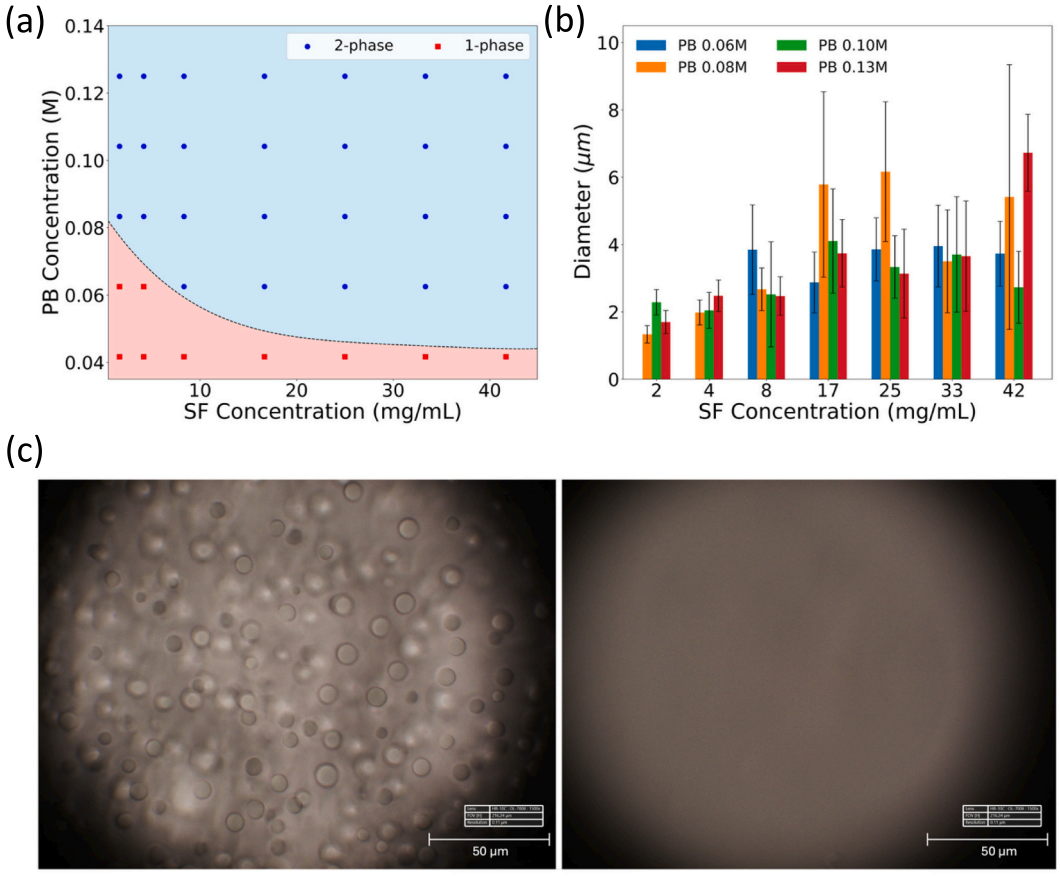

Fig. 3. (a) Phase diagram of the SF + PB system obtained from microscopy experiments (b) Dense phase droplets size distribution in liquid phase. Bars represent the average, whiskers correspond to standard deviation. (c) Optical images of SF + PB coacervates before (left panel) and after (right panel) the addition of HDO, showing the disappearance of phase separation.

Different results were obtained in the tests with NaCl, ATP and urea, as shown in Fig. S2. This, reminiscent of what was reported for SF in the presence of an anionic surfactant [47], corroborates that phase separation is driven mainly by hydrophobic interactions.

Circular dichroism was performed to get insight into the secondary structure of the protein. In Fig. 4a, the CD spectra are depicted for both SF and SF + PB. Our analysis, in accordance with previous findings, showed that regenerated silk fibroin in aqueous solutions is mainly in

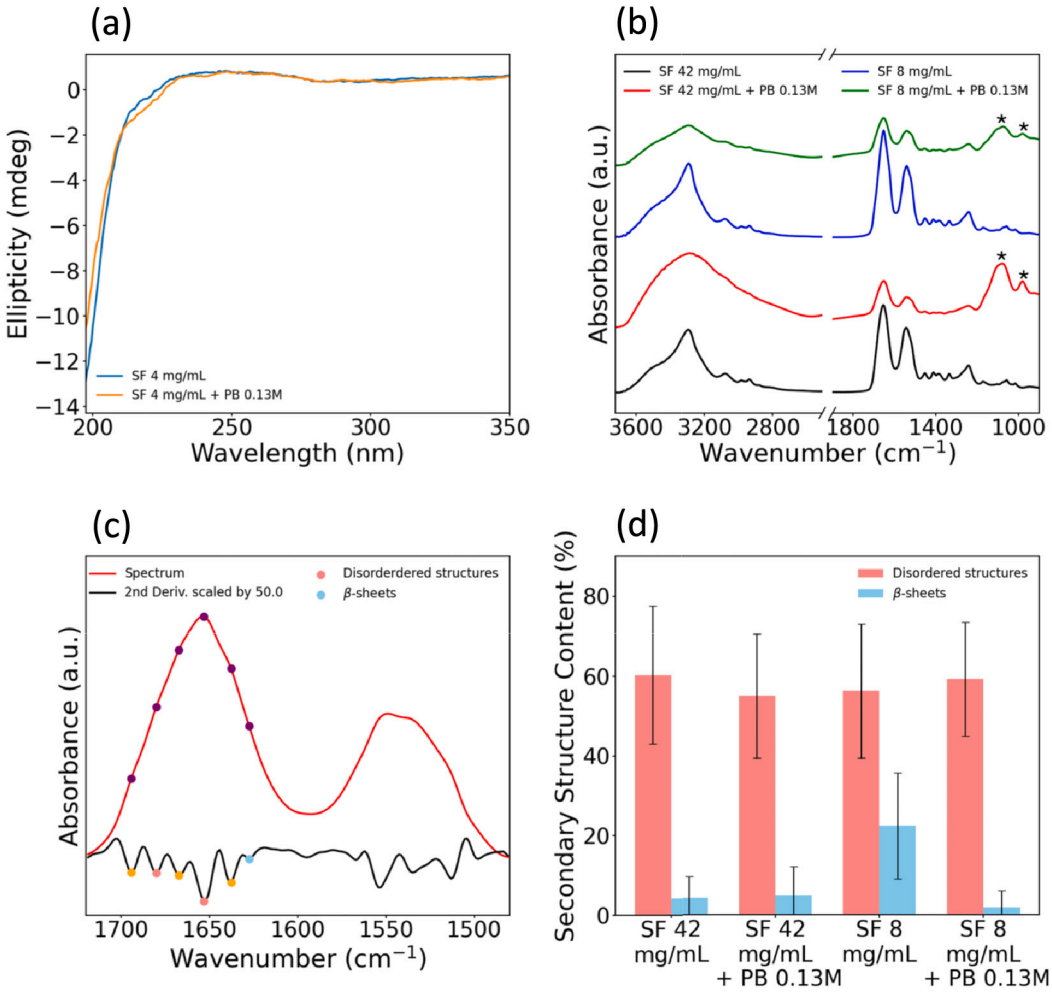

Fig. 4. Analysis of the secondary structure of SF in solution and after drying. (a) Circular dichroism spectra of SF 4 mg/mL, and SF 4 mg/mL + PB 0.13 M solutions. (b) Mean FTIR spectra of the SF and SF + PB films obtained from solutions with different SF concentrations, calculated from the micro-FTIR maps. (c) Example of secondary structures peak assignments in the Amide *I* band, based on the second derivative of the absorbance spectrum. The depicted spectrum comes from one of the SF 42 mg/mL maps. (d) Behavior of secondary structure components for the SF and SF + PB films extracted from the micro-FTIR maps. Data are plotted as mean +/− standard deviation.

random coil conformation, as evidenced by the large negative decreasing behavior of the ellipticity while approaching 200 nm [50,51]. This result is confirmed for the SF + PB sample, showing that it is likely that secondary structure of the protein remains unchanged after SF undergoes LLPS.

Similar results were obtained when we looked at the conformation of SF in the dried films via micro-FTIR. In those spectra, the fingerprint region for protein conformation is conventionally elected as Amide I and II bands, at 1600–1700 and 1470–1570 cm^{-1}, respectively. The comparison of the mean spectra in Fig. 4b evidence that, in both SF samples (8 mg/mL and 42 mg/mL), the Amide I and Amide II features peak around 1655 cm^{-1} and 1541 cm^{-1}, respectively. The addition of PB, whose characteristic signals arise at 985 and 1088 cm^{-1} (asterisks), does not induce any detectable changes in band shape, indicating that SF secondary structure is preserved. This observation is further supported by second derivative analysis of the spectral profiles (Fig. 4c and d) and it is consistent with the CD results: no statistically significant rearrangement is observed upon LLPS formation, indicating that SF maintains a similar secondary structure, predominantly random-coil, in both the protein light and dense separated phases. This status quo persists even after extensive solvent evaporation as observed in the resulting films.

Consistently, the dried films tend to contain mainly disordered structures, similar to the conformation of the protein in solution. This indicates that the condensation of SF into coacervates by phosphate addition does not alter the secondary structure of SF, either in solution, or in dried films.

A modeling approach was carried out to get further comprehension of the system. The detailed description of the model is presented in the Materials and Methods section. In Fig. 5a there is a representation of the simulated SF chain, with the attractive beads being the blue and red ones. Simulations have been launched varying only 2 parameters: (i) the size of the cubic box, adjusted to reproduce the experimental concentrations under the hypothesis that the SF chain molecular weight equals the average molecular weight of the silk solution, and (ii) the value of ε_B (and consequently ε_R, since it has been fixed to ε_B /2), which is the intensity of the Lennard-Jones attractive well. This parameter was varied to mimic the increased hydrophobic interaction among the SF chains caused by the addiction of the kosmotropic phosphate anions. The repulsive interactions among the chains are accounted only with an excluded volume WCA potential with parameters fixed among different simulations. The model successfully captures the behavior of the protein, as by varying ε_B we can go from a situation where the chains are dispersed in the box, condition that represents the homogeneous solution, to one where some of them start creating a cluster, meaning that phase separation has occurred. In Fig. 5b and c, these two conditions are

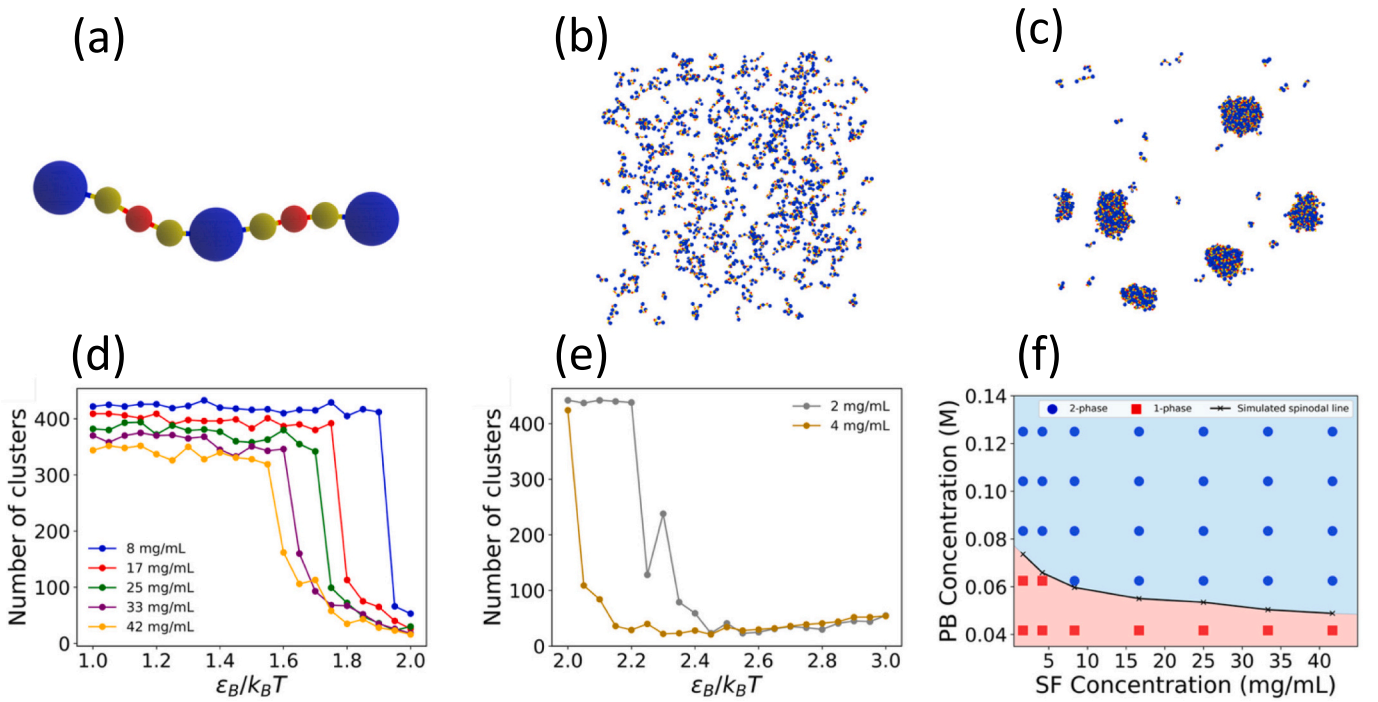

Fig. 5. Computational model for the phase behavior of silk and its self-assembly characterization. (a) Schematic representation of the model. (b) Final configuration showing no LLPS. SF concentration is 25 mg/mL, and $\varepsilon_B = 1.3\ k_BT$ (c) Final configuration showing the occurrence of LLPS. SF concentration is 25 mg/mL, and $\varepsilon_B = 2k_BT$ (d) Number of clusters at the end of each simulation, as function of ε_B, for concentrations of SF equal to 8 mg/mL, 17 mg/mL, 25 mg/mL, 33 mg/mL, 42 mg/mL. (e) Number of clusters at the end of each simulation, as function of ε_B, for concentrations of SF equal to 2 mg/mL and 4 mg/mL. (f) Superposition of the model prediction on the experimental phase diagram by linear rescaling. Errors on the points of the simulated spinodal line are not depicted since they're smaller than the size of the markers.

depicted. To quantitatively determine whether the phase separation had happened at the end of the simulation, we defined the parameters N_{clus} as the total number of clusters in the box. Two SF chains are defined to be in the same cluster if there is any non-bonded attractive interaction among two or more beads of the chains. In this way, the occurrence of LLPS is observed when there is a steep decrease of N_{clus}. The behavior of N_{clus} with ε_B is represented in Fig. 5d and e, for all the SF concentrations tested. In this way, we can define the simulated critical depth of the well ε_B^* as function of the SF concentration. The model clearly mimics the experimental data of the phase diagram, presented in Fig. 1e, where less concentrated phosphate solution is needed at higher concentrations of SF to obtain the phase separation. To be able to compare the experimental results with the simulations we observed that, as reported in the literature [52], the salting out effect of the kosmotropic phosphate ions that drives the LLPS in silk protein systems is mainly an entropic effect. In view of this, we performed a linear rescaling of the critical well depth ε_B^* on the concentration of PB from the phase diagram, following the Asakura-Oosawa theory of depletion interactions [53]. This operation led to good agreement between the simulations and the experimental phase diagram, as reported in Fig. 5f, confirming the ability of the model to explain the tendency of the system to undergo LLPS. Moreover, the liquidity of the protein chains in the clusters was characterized by means of the radial distribution function between the B beads, similarly to what was done by Lemetti et al. [36]; the results are reported in the Supplementary information, Fig. S3. They observed that, from the simulations' point of view, one of the main difference between solid (which they refer to as "aggregates") against liquid ones (which they call by the term "coacervates") relies on the persistency of spatial correlations among the beads, as in coacervates they extend to practically the full length scale represented in the simulation. We observed a similar behavior in our case, hinting towards the fact that a liquid phase is forming rather than a solid one. We believe that this model represents a simple yet effective starting point for describing the properties of SF protein explored via the experimental characterizations carried out in the work, in particular the phase diagram. Further analyses, which are currently in progress and will be the subject of a future study, will be needed to assess the range of applicability of the model presented here.

It is well known that alcohols cause conformational transition of silk fibroin from random coil to β-sheet crystalline structure, leading to gel formation. Several studies [54,55] clarified that the SF crystallization mechanism can be described by the polar groups of alcohols pulling water away from silk fibroin molecules, resulting in increased aggregation of hydrophobic amino acids with the polarity being tuned by the length of alcohol carbon chain. Hence, ethanol is expected to promote gelation of silk fibroin via β-sheet crystallization. Fig. 6a shows that after ethanol treatment the phase separation is still present, and particles with similar sizes are stabilized into the SF matrix. The size comparison among the stabilized particles is represented in Fig. S4 (see Supplementary information). Fig. 6b and shows the mean FTIR spectra of the SF (42 mg/mL) and SF (42 mg/mL) + PB (0.13 M) films after ethanol treatment. A marked increase in β-sheet content is observed respect to the non-treated samples, as indicated by the enhanced contributions at 1628 cm^{-1} and 1694 cm^{-1} (dashed lines) in the Amide I region, compared to the untreated SF films (Fig. 4 b–d). A magnified view of the Amide bands for one sample, as long as the second derivative spectra used for the analysis of the secondary structure, is shown in Supplementary information, Fig. S5. The increase in β-sheets content resulted from the hydrophobic interaction between silk fibroin protein chains and additional alcohols.

Gel fractions can be used to measure the insoluble part of silk-fibroin films by the gravimetric method, consisting in the calculation of the mass percentage ratio between the initial sample and dried film, after the immersion in simulated body fluids. Without the addition of ethanol, SF and SF + PB dissolve rapidly both in gastric and intestinal body fluids (see Movies S2-S5). On the other hand, it was found that the gel fraction increased after ethanol treatment (Fig. 6c). This finding is in good

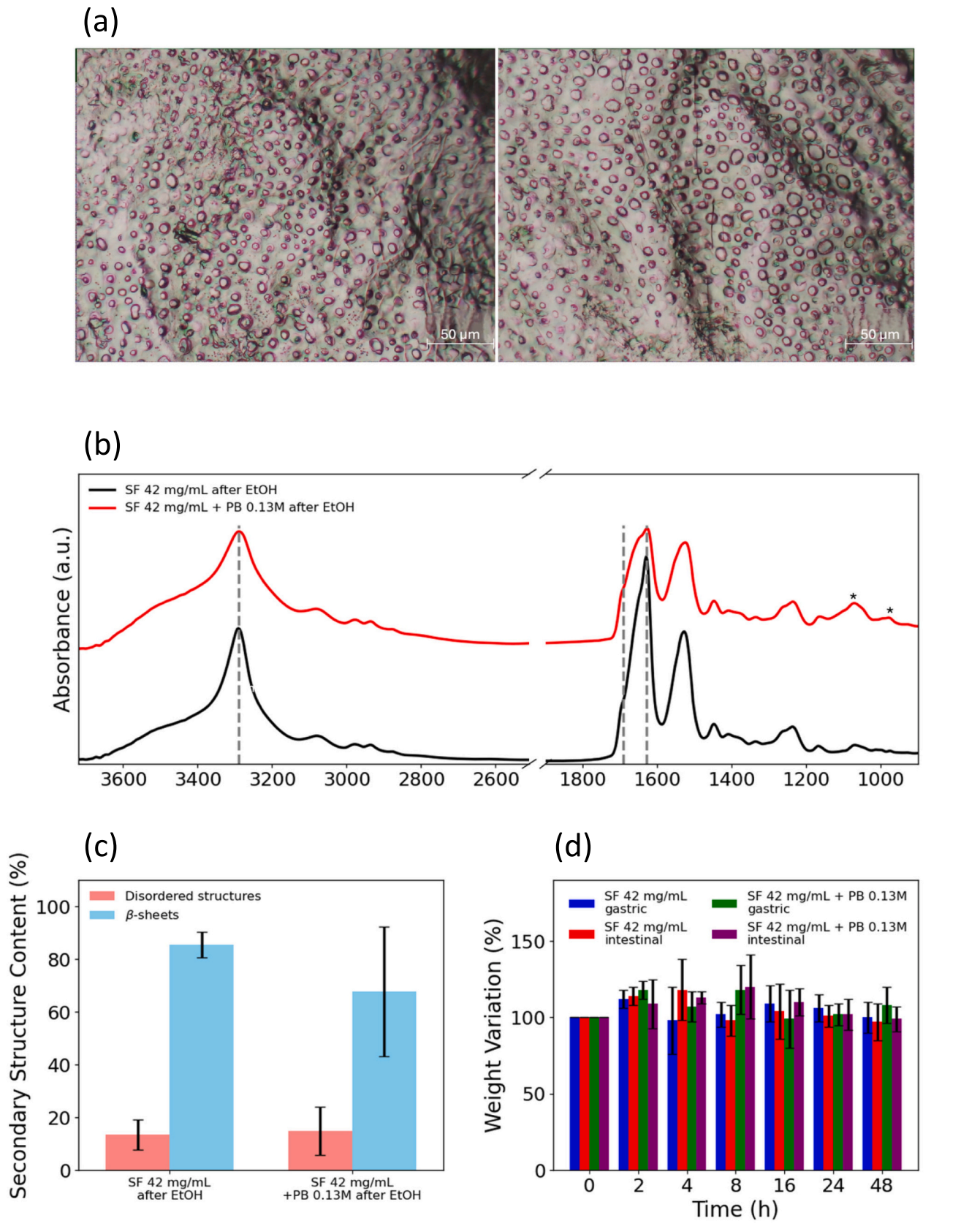

Fig. 6. (a) Micrographs of LLPS systems in dried films after ethanol treatment (SF 42 mg/mL (left panel) and SF 42 mg/mL + PB 0.13 M (right panel)). (b) Average FTIR spectra of the SF and SF 42 mg/mL + PB 0.13 M films after ethanol treatment. (c) Secondary structures components for the SF and SF 42 mg/mL + PB 0.13 M films extracted from the micro-FTIR maps. (d) Data of the dissolution test of SF and SF 42 mg/mL + PB 0.13 M in 0.1 M HCl (gastric), and subsequentially in the K_2HPO_4/KH_2PO_4 (intestine) buffer solution.

agreement with the mechanical strength of silk fibroin films that also increased with the increasing amount of carbon atoms in monohydric alcohol [56]. This, confirmed by FTIR spectra, is related to the conformational structure of the silk fibroin itself after ethanol evaporation. The polarity of alcohol caused some degree of β-sheet crystallization that promoted physical crosslinks in the silk structure, resulting in gel formation. Moreover, treatment with ethanol greatly enhances the physical and chemical stability of the material. In fact, while for untreated SF and SF + PB films rapid dissolution was observed for both gastric and intestinal simulated fluids, ethanol-treated films showed good performances up to 48 h in both media (Fig. 6d).

4. Conclusions

This work demonstrates that phosphate anions can trigger liquid–liquid phase separation (LLPS) in silk fibroin (SF) aqueous solutions. Phosphate-induced LLPS proceeds through enhancement of hydrophobic interactions between SF chains. This was consistently validated by experimental evidence and corroborated by coarse-grained bead–spring simulations, providing a molecular-level interpretation of the observed assembly behavior. The phase diagram of SF was constructed by varying the concentrations of SF and PB to determine the minimum PB concentration required for LLPS.

Spectroscopic analyses confirm that SF within the phase-separated droplets predominantly retains a random coil conformation, demonstrating that LLPS occurs independently of premature β-sheet formation. During solvent evaporation, SF-rich droplets become spatially confined within a continuous silk matrix, yielding a hierarchical material architecture. Subsequent ethanol treatment effectively stabilizes this structure by inducing β-sheet formation, resulting in structurally stable materials.

The resulting SF formulations performance in simulated biological fluids revealed pronounced pH-dependent stability profiles. Together, these findings establish phosphate-mediated LLPS as tunable, biomimetic, and versatile strategy for directing SF self-assembly. This approach expands the toolbox for silk-based material design and paves the way for the development of advanced biomedical and pharmaceutical systems with programmable structure and functionality.

Despite the insights provided, this study holds some limitations that should be acknowledged. In particular, the experimental conditions and coarse-grained modeling approach do not capture the full physiological complexity of *Bombyx mori* silk gland, including complete ionic environment, concentration gradients, shear forces, and dynamic spatiotemporal regulation present during natural spinning. Moreover, while the stability of LLPS-derived films was evaluated in simulated biological fluids, long-term degradation and *in vivo* behavior were not addressed and do warrant future investigation.

CRediT authorship contribution statement

Rocco Malaspina: Writing – review & editing, Software, Investigation, Data curation. **Martina Alunni Cardinali:** Writing – review & editing, Investigation, Data curation. **Danila Maltsev:** Writing – review & editing, Investigation. **Valeria Libera:** Writing – review & editing, Methodology, Investigation. **Alessia Pepe:** Investigation, Data curation. **Lucia Comez:** Writing – review & editing, Methodology, Funding acquisition. **Cristiano De Michele:** Writing – review & editing, Software. **Caterina Petrillo:** Writing – review & editing, Funding acquisition. **Alessandro Paciaroni:** Writing – review & editing, Supervision, Funding acquisition, Conceptualization. **Paola Sassi:** Writing – review & editing, Supervision, Methodology. **Luca Valentini:** Writing – original draft, Supervision, Funding acquisition, Conceptualization.

Funding

L.V., P.S., M.A.C., A.P. and L.C. acknowledge the Italian Ministry of University and Research (MUR) National Innovation Ecosystem grant ECS00000041-VITALITY-CUP J97G22000170005 and CUP B43C22000470005.

Declaration of competing interest

The authors declare the following financial interests/personal relationships which may be considered as potential competing interests:

Alessandro Paciaroni reports financial support was provided by University of Perugia. If there are other authors, they declare that they have no known competing financial interests or personal relationships that could have appeared to influence the work reported in this paper.

Acknowledgments

The authors kindly aknowledge Prof. M. Dindo from the University of Perugia for supplying us ATP. Prof. P. Mariani – Polytechnic University of Marche is also acknowledged for the availability of the instrumentation for FRAP experiments.

Appendix A. Supplementary data

Supplementary data to this article can be found online at https://doi.org/10.1016/j.ijbiomac.2026.152622.

Data availability

Data will be made available on request.

References

[1] W. Qiu, A. Patil, F. Hu, X.Y. Liu, Hierarchical structure of silk materials versus mechanical performance and mesoscopic engineering principles, Small 15 (2019).
[2] Q. Wang, S. Ling, Q. Yao, Q. Li, D. Hu, Q. Dai, D.A. Weitz, D.L. Kaplan, M. J. Buehler, Y. Zhang, Observations of 3 nm silk nanofibrils exfoliated from natural silkworm silk fibers, ACS Mater. Lett. 2 (2020) 153–160, https://doi.org/10.1021/acsmaterialslett.9b00461.
[3] Y.X. He, N.N. Zhang, W.F. Li, N. Jia, B.Y. Chen, K. Zhou, J. Zhang, Y. Chen, C. Z. Zhou, N-terminal domain of Bombyx Mori fibroin mediates the assembly of silk in response to PH decrease, J. Mol. Biol. 418 (2012) 197–207, https://doi.org/10.1016/j.jmb.2012.02.040.
[4] X. Wang, H.J. Kim, P. Xu, A. Matsumoto, D.L. Kaplan, Biomaterial coatings by stepwise deposition of silk fibroin, Langmuir 21 (2005) 11335–11341, https://doi.org/10.1021/la051862m.
[5] X. Chen, D.P. Knight, Z. Shao, β-Turn formation during the conformation transition in silk fibroin, Soft Matter 5 (2009) 2777–2781, https://doi.org/10.1039/b900908f.
[6] C.W.P. Foo, E. Bini, J. Hensman, D.P. Knight, R.V. Lewis, D.L. Kaplan, Role of PH and charge on silk protein assembly in insects and spiders, Appl. Phys. A Mater. Sci. Process. 82 (2006) 223–233, https://doi.org/10.1007/s00339-005-3426-7.
[7] A.S. Lammel, X. Hu, S.H. Park, D.L. Kaplan, T.R. Scheibel, Controlling silk fibroin particle features for drug delivery, Biomaterials 31 (2010) 4583–4591, https://doi.org/10.1016/j.biomaterials.2010.02.024.
[8] Y. Han, S. Wang, Y. Cao, G.P. Singh, S.I. Loh, R. Cheerlavancha, M.C.Y. Ang, D. T. Khong, P.W.L. Chua, P. Ho, et al., Design of biodegradable, climate-specific packaging materials that sense food spoilage and extend shelf life, ACS Nano 17 (2023) 8333–8344, https://doi.org/10.1021/acsnano.2c12747.
[9] Y. Wang, L. Li, Y.E. Ji, T. Wang, Y. Fu, X. Li, G. Li, T. Zheng, L. Wu, Q. Han, et al., Silk-protein-based gradient hydrogels with multimode reprogrammable shape changes for biointegrated devices, Proc. Natl. Acad. Sci. USA 120 (2023), https://doi.org/10.1073/pnas.2305704120.
[10] I.C.M. Candido, G. da S. Oliveira, S.J.L. Ribeiro, M. Cavicchioli, H.S. Barud, L. G. Silva, H.P. de Oliveira, PVA-silk fibroin bio-based triboelectric nanogenerator, Nano Energy 105 (2023), https://doi.org/10.1016/j.nanoen.2022.108035.
[11] H. Wang, M. Jian, S. Li, X. Liang, H. Lu, K. Xia, M. Zhu, Y. Wu, Y. Zhang, Inter-Shell sliding in individual few-walled carbon nanotubes for flexible electronics, Adv. Mater. 35 (2023), https://doi.org/10.1002/adma.202306144.
[12] D. Lin, M. Li, L. Wang, J. Cheng, Y. Yang, H. Wang, J. Ye, Y. Liu, Multifunctional hydrogel based on silk fibroin promotes tissue repair and regeneration, Adv. Funct. Mater. 34 (2024).
[13] T.D. Fink, R.H. Zha, Silk and silk-like supramolecular materials, Macromol. Rapid Commun. 39 (2018).
[14] X. Yao, S. Zou, S. Fan, Q. Niu, Y. Zhang, Bioinspired silk fibroin materials: from silk building blocks extraction and reconstruction to advanced biomedical applications, Mater. Today Bio 16 (2022).
[15] C. Fu, Z. Shao, V. Fritz, Animal silks: their structures, properties and artificial production, Chem. Commun. (2009) 6515–6529.

[16] L. Römer, T. Scheibel, The elaborate structure of spider silk: structure and function of a natural high performance Fiber, Prion 2 (2008) 154–161.
[17] C. Jiang, X. Wang, R. Gunawidjaja, Y.H. Lin, M.K. Gupta, D.L. Kaplan, R.R. Naik, V. V. Tsukruk, Mechanical properties of robust ultrathin silk fibroin films, Adv. Funct. Mater. 17 (2007) 2229–2237, https://doi.org/10.1002/adfm.200601136.
[18] M.G. Lay, N.A. Oktaviani, A.D. Malay, K. Numata, Exploring the self-assembly of silk proteins through liquid-liquid phase separation, Polym. J. 57 (2025) 799–814.
[19] S. Yang, K.H. Lee, Spontaneous hollow coacervate transition of silk fibroin via dilution and its transition to microcapsules, Biomacromolecules 26 (2025) 2513–2528, https://doi.org/10.1021/acs.biomac.5c00003.
[20] S. Yang, Y. Yu, S. Jo, Y. Lee, S. Son, K.H. Lee, Calcium ion-triggered liquid-liquid phase separation of silk fibroin and spinning through acidification and shear stress, Nat. Commun. 15 (2024), https://doi.org/10.1038/s41467-024-54588-1.
[21] R. Fan, K. Knuuttila, B. Schmuck, G. Greco, A. Rising, M.B. Linder, A.S. Aranko, Sustainable spinning of artificial spider silk fibers with excellent toughness and inherent potential for functionalization, Adv. Funct. Mater. 35 (2025), https://doi.org/10.1002/adfm.202410415.
[22] M. Landreh, H. Osterholz, G. Chen, S.D. Knight, A. Rising, A. Leppert, Liquid-liquid crystalline phase separation of spider silk proteins, Commun. Chem. 7 (2024), https://doi.org/10.1038/s42004-024-01357-2.
[23] A. Leppert, G. Chen, D. Lama, C. Sahin, V. Railaite, O. Shilkova, T. Arndt, E. G. Marklund, D.P. Lane, A. Rising, et al., Liquid-liquid phase separation primes spider silk proteins for Fiber formation via a conditional sticker domain, Nano Lett. 23 (2023) 5836–5841, https://doi.org/10.1021/acs.nanolett.3c00773.
[24] A. Barrett, J. Imbrogno, G. Belfort, P.B. Petersen, Phosphate ions affect the water structure at functionalized membrane surfaces, Langmuir 32 (2016) 9074–9082, https://doi.org/10.1021/acs.langmuir.6b01936.
[25] M.G. Cacace, E.M. Landau, J.J. Ramsden, The Hofmeister series: salt and solvent effects on interfacial phenomena, Q. Rev. Biophys. 30 (1997) 241–277.
[26] V. Yeh, J.M. Broering, A. Romanyuk, B. Chen, Y.O. Chernoff, A.S. Bommarius, The Hofmeister effect on amyloid formation using yeast prion protein, Protein Sci. 19 (2010) 47–56, https://doi.org/10.1002/pro.281.
[27] A.C. Dumetz, A.M. Snellinger-O'Brien, E.W. Kaler, A.M. Lenhoff, Patterns of protein–protein interactions in salt solutions and implications for protein crystallization, Protein Sci. 16 (2007) 1867–1877, https://doi.org/10.1110/ps.072957907.
[28] T.D. Fink, J.L. Funnell, R.J. Gilbert, R.H. Zha, One-pot assembly of drug-eluting silk coatings with applications for nerve regeneration, ACS Biomater. Sci. Eng. 10 (2024) 482–496, https://doi.org/10.1021/acsbiomaterials.3c01042.
[29] A.M. Ziemba, T.D. Fink, M.C. Crochiere, D.L. Puhl, S. Sapkota, R.J. Gilbert, R. H. Zha, Coating topologically complex electrospun fibers with nanothin silk fibroin enhances neurite outgrowth in vitro, ACS Biomater. Sci. Eng. 6 (2020) 1321–1332, https://doi.org/10.1021/acsbiomaterials.9b01487.
[30] R.H. Zha, P. Delparastan, T.D. Fink, J. Bauer, T. Scheibel, P.B. Messersmith, Universal nanothin silk coatings: via controlled spidroin self-assembly, Biomater. Sci. 7 (2019) 683–695, https://doi.org/10.1039/c8bm01186a.
[31] C. Wigham, T.D. Fink, M. Sorci, P. O'Reilly, S. Park, J. Kim, V.R. Varude, R.H. Zha, Phosphate-driven interfacial self-assembly of silk fibroin for continuous noncovalent growth of Nanothin defect-free coatings, ACS Appl. Mater. Interfaces 16 (2024) 58121–58134, https://doi.org/10.1021/acsami.4c07528.
[32] Q.A. Besford, M. Liu, A. Gray-Weale, Pair correlations that link the hydrophobic and Hofmeister effects, Phys. Chem. Chem. Phys. 18 (2016) 14949–14959, https://doi.org/10.1039/c5cp05132k.
[33] J.A. Joseph, J.R. Espinosa, I. Sanchez-Burgos, A. Garaizar, D. Frenkel, R. Collepardo-Guevara, Thermodynamics and kinetics of phase separation of protein-RNA mixtures by a minimal model, Biophys. J. 120 (2021) 1219–1230, https://doi.org/10.1016/j.bpj.2021.01.031.
[34] J.-M. Choi, A.S. Holehouse, R.V. Pappu, Physical principles underlying the complex biology of intracellular phase transitions BB49CH06_Pappu ARjats.Cls 46 (2026) 30, https://doi.org/10.1146/annurev-biophys-121219.
[35] G.L. Dignon, R.B. Best, J. Mittal, 37 Annual Review of Physical Chemistry Downloaded from www.annualreviews.org. Guest (Guest) IP: 193.48.115.61 On: Tue vol. 9, 2026, p. 50, https://doi.org/10.1146/annurev-physchem-071819.
[36] L. Lemetti, A. Scacchi, Y. Yin, M. Shen, M.B. Linder, M. Sammalkorpi, A.S. Aranko, Liquid-liquid phase separation and assembly of silk-like proteins is dependent on the polymer length, Biomacromolecules 23 (2022) 3142–3153, https://doi.org/10.1021/acs.biomac.2c00179.
[37] C.Z. Zhou, F. Confalonieri, M. Jacquet, R. Perasso, Z.G. Li, J. Janin, Silk fibroin: structural implications of a remarkable amino acid sequence, Proteins Struct. Funct. Genet. 44 (2001) 119–122, https://doi.org/10.1002/prot.1078.
[38] H.Y. Wang, Y.Q. Zhang, Effect of regeneration of liquid silk fibroin on its structure and characterization, Soft Matter 9 (2013) 138–145, https://doi.org/10.1039/c2sm26945g.
[39] H. Yamada, H. Nakao, Y. Takasu, K. Tsubouchi, Preparation of Undegraded Native Molecular Fibroin Solution from Silkworm Cocoons Vol. 14, 2001.
[40] J. Wang, J.M. Choi, A.S. Holehouse, H.O. Lee, X. Zhang, M. Jahnel, S. Maharana, R. Lemaitre, A. Pozniakovsky, D. Drechsel, et al., A molecular grammar governing the driving forces for phase separation of prion-like RNA binding proteins, Cell 174 (2018) 688–699.e16, https://doi.org/10.1016/j.cell.2018.06.006.
[41] D.J. Belton, R. Plowright, D.L. Kaplan, C.C. Perry, A robust spectroscopic method for the determination of protein conformational composition – application to the annealing of silk, Acta Biomater. 73 (2018) 355–364, https://doi.org/10.1016/j.actbio.2018.03.058.
[42] A.D. Malay, T. Suzuki, T. Katashima, N. Kono, K. Arakawa, K. Numata, Spider Silk Self-assembly Via Modular Liquid-Liquid Phase Separation and Nanofibrillation Vol. 6, 2020.
[43] S. Alberti, P. Arosio, R.B. Best, S. Boeynaems, D. Cai, R. Collepardo-Guevara, G. L. Dignon, R. Dimova, S. Elbaum-Garfinkle, N.L. Fawzi, et al., Current practices in the study of biomolecular condensates: a community comment, Nat. Commun. 16 (2025).
[44] U.K. Slotta, S. Rammensee, S. Gorb, T. Scheibel, An engineered spider silk protein forms microspheres, Angew. Chem. Int. Ed. 47 (2008) 4592–4594, https://doi.org/10.1002/anie.200800683.
[45] G. Krainer, T.J. Welsh, J.A. Joseph, J.R. Espinosa, S. Wittmann, E. de Csilléry, A. Sridhar, Z. Toprakcioglu, G. Gudiškytė, M.A. Czekalska, et al., Reentrant liquid condensate phase of proteins is stabilized by hydrophobic and non-ionic interactions, Nat. Commun. 12 (2021), https://doi.org/10.1038/s41467-021-21181-9.
[46] T. Zheng, N. Wake, S.L. Weng, T.M. Perdikari, A.C. Murthy, J. Mittal, N.L. Fawzi, Molecular insights into the effect of 1,6-Hexanediol on FUS phase separation, EMBO J. 44 (2025) 2725–2740, https://doi.org/10.1038/s44318-025-00431-2.
[47] R. Zhu, R. Wang, J. Li, M. Chen, L. Qiu, S. Bai, An artificial liquid–liquid phase separation-driven silk fibroin-based adhesive for rapid hemostasis and wound sealing, Acta Biomater. 182 (2024) 14–27, https://doi.org/10.1016/j.actbio.2024.05.024.
[48] Y. Wu, L. Qiu, X. Ou, J. Tao, M. Zheng, Y. Huang, S. Bai, Injectable silk fibroin-based hydrogels with ultrafast in situ gelation via an unfolding-aggregating strategy for osteoarthritis treatment, Biomacromolecules 26 (2025) 7447–7469, https://doi.org/10.1021/acs.biomac.5c01002.
[49] S. Cao, G. Li, P. Zhou, E. Gazit, X. Yan, C. Yuan, Entropy-driven amino acid-based coacervates with enzyme-free metabolism and prebiotic robustness, J. Am. Chem. Soc. 147 (2025) 45324–45336, https://doi.org/10.1021/jacs.5c15328.
[50] S. Lee, S.H. Kim, Y.Y. Jo, W.T. Ju, H.B. Kim, H.Y. Kweon, Conformation transition kinetics of silk fibroin in aqueous solution explored using circular dichroism spectroscopy, ChemistrySelect 6 (2021) 1735–1740, https://doi.org/10.1002/slct.202004180.
[51] V. Libera, R. Malaspina, S. Bittolo Bon, M.A. Cardinali, I. Chiesa, C. De Maria, A. Paciaroni, C. Petrillo, L. Comez, P. Sassi, et al., Conformational transitions in redissolved silk fibroin films and application for printable self-powered multistate resistive memory biomaterials, RSC Adv. 14 (2024) 22393–22402, https://doi.org/10.1039/d4ra02830a.
[52] R. Zangi, M. Hagen, B.J. Berne, Effect of ions on the hydrophobic interaction between two plates, J. Am. Chem. Soc. 129 (2007) 4678–4686, https://doi.org/10.1021/ja068305m.
[53] S. Asakura, F. Oosawa, On interaction between two bodies immersed in a solution of macromolecules, J. Chem. Phys. 22 (1954) 1255–1256.
[54] I.C. Um, H.Y. Kweon, K.G. Lee, Y.H. Park, The role of formic acid in solution stability and crystallization of silk protein polymer, Int. J. Biol. Macromol. 33 (2003) 203–213, https://doi.org/10.1016/j.ijbiomac.2003.08.004.
[55] K. Kaewprasit, T. Kobayashi, S. Damrongsakkul, Thai silk fibroin gelation process enhancing by monohydric and polyhydric alcohols, Int. J. Biol. Macromol. 118 (2018) 1726–1735, https://doi.org/10.1016/j.ijbiomac.2018.07.017.
[56] S. Kaewpirom, S. Boonsang, Influence of alcohol treatments on properties of silk-fibroin-based films for highly optically transparent coating applications, RSC Adv. 10 (2020) 15913–15923, https://doi.org/10.1039/d0ra02634d.